Mathematical Biosciences and Engineering

MBE, 18(4): 4358–4371.
DOI: 10.3934/mbe.2021219
Received: 09 March 2021
Accepted: 21 April 2021
Published:19 May 2021

http://www.aimspress.com/journal/MBE

Research article

Two dimensional automatic active shape model of degenerative disc repaired by low-intensity laser

Ming Huang, Wenfei Dong*, Yingjie Sun and Baowen He

Department of Anesthesiology, General Hospital of Northern Theater, Shenyang 110016, China

*** Correspondence:** Email: dongwf3144@sina.com.

Abstract: *Objective:* Intervertebral disc degeneration is the main factor causing low back pain, and the related long-term treatment can improve the situation of degeneration. This study aimed to investigate the effect of low-intensity laser irradiation on the repair of degenerative intervertebral disc by two dimensional automatic active shape model (2D-AASM). *Methods:* Nine Bama miniature pigs were randomly divided into three groups: control group (Con), model group (Mod) and laser treatment group (Las). After one month, the discs were treated with low-energy laser for another month. MRI was performed for one month, and the statistical shape model and 2D-AASM of intervertebral disc were established based on the minimum description length method. *Results:* The model established by the proposed method is more accurate and the segmentation result is more accurate. From the segmented T2-weighted image, the signal intensity of the Mod group decreased significantly, and the signal intensity in the Las group was moderate and high compared with the Mod group. The HE staining display the structure of Con group was damaged, and the construction of Las group was restored compared with Mod group. *Conclusions:* The 2D-AASM method effectively improves the accuracy of intervertebral disc segmentation. The low-intensity laser has a protective effect on the repair of the degenerative intervertebral disc.

Keywords: low-intensity laser; intervertebral disc segmentation; bama miniature pigs; magnetic resonance imaging; active shape model

1. Introduction

Spinal disease has become one of the major diseases affecting public health. Intervertebral disc segmentation technology is very important for spinal magnetic resonance image (MRI)

processing [1–3]. Accurate and efficient segmentation of the intervertebral disc is not only conducive to shorten the time consumed by doctors in the diagnosis of spinal diseases, but also can assist in the treatment of spinal diseases by calculating the parameters of the intervertebral disc [4]. There are 23 intervertebral discs in the human body. If we use the manual segmentation method, it will be very time-consuming. At the same time, different operators will also lead to subjective differences in the segmentation results. However, the computer quantitative processing of MRI images can improve the efficiency of spine diagnosis and overcome the subjective differences [5].

Low back pain is one of the common orthopedic diseases. Its incidence rate is increasing and showing a trend of younger age and seriousness. Intervertebral disc degeneration is the main cause of low back pain [6,7]. The disc is mainly composed of fibrous rings, nucleus pulposus and upper and lower endplates, in which the nucleus pulposus is surrounded by fibrous rings rich in water. The moisture content of nucleus pulposus is higher than that of annulus fibrous rings. The moisture content of nucleus pulposus is about 95% at birth, 80% at infancy and 70% at old age. Studies have shown that [8], the cartilage endplate of the intervertebral disc begins to degenerate in 2-year-old children. At present, the factors leading to disc degeneration are not completely clear. When the disc degenerates, the fibrous ring and nucleus pulposus degenerate one after another, the dehydration and water absorption function of nucleus pulposus weaken, the volume decreases, and the elasticity decreases. One of the characteristics of disc degeneration is the decrease of water content.

Aquaporin-1 (AQP-1) has been found and confirmed by American scientists [9], Obvious correlation had been found between the AQP-1 and intervertebral disc degeneration. The decrease of AQP-1 in intervertebral disc will decrease the water content and the permeability of nutrients, affect the nutrition supply of intervertebral disc, and then affect the cell function, leading to the degeneration of intervertebral disc [10]. Other studies also show that AQP-1 is closely related to disc degeneration [11–13].

The purpose of this study is to investigate the effect of low intensity laser irradiation on the repair of degenerative intervertebral disc by two dimensional automatic active shape model (2D-AASM), and to provide a reliable experimental basis for the treatment of disc herniation with low intensity laser technology.

2. Materials and methods

2.1. Animals and groups

Nine healthy adult Bama pigs, male and female, weighing 50–60 kg, were provided by the Medical Laboratory Animal Department of Shenyang Military General Hospital. According to the random number table method, the Bama pigs were randomly divided into three groups, three in each group, which were control group (Con group), model group (Mod group) and laser treatment group (Las group). The con group was observed for 2 months without any experimental treatment. In the mod group, the model of intervertebral disc degeneration was established and then observed for another 2 months. In the Las group, the model of intervertebral disc degeneration was established and observed for one month, and the model was treated with low-energy laser for another month. The study was approved by the ethics committee General Hospital of Northern Theater.

2.2. Establishment and treatment of model

Before the operation, the vein access was established by the ear vein puncture, and 3 mg/kg

propofol was given intravenously for anesthesia. After anesthesia, the small Bama pig was lying on the left lateral position with C-arm X-ray guidance, and propofol 8 mL/h was continuously pumped to maintain anesthesia, and vital signs were monitored during the operation. During the operation, normal saline was infused intravenously and 1.6 million units of penicillin were given to prevent infection.

The model of intervertebral disc degeneration was made. Under the guidance of C arm X-ray, the intervertebral space of L2-3, L3-4, L4-5 and L5-6 were determined. Then 1% lidocaine was used for infiltration anesthesia, and 16 G guide needle was used to puncture the intervertebral disc along the location point. After penetrating the posterior side of the fibrous rings, the disc was damaged radially by acupuncture. After the operation, 800,000 units of penicillin were used for 3 consecutive days, and the defecation and diet of each day were observed. One week later, the dressing was removed and one month later MR was performed to verify the success of the model.

One month after the success of the model, low-intensity laser treatment was carried out on the intervertebral disc. Under the guidance of C arm X-ray, after the needle tip position is correct, a straight puncture needle is introduced into the middle of the intervertebral disc along the guide needle. A fiber with an outer diameter of 400 μm is introduced into the puncture needle. The fiber is connected to the laser equipment. The laser power is set to 3 watts, and the preset energy is 900 joules. Laser radiation time (exposure time) is 30 seconds. The laser radiation intensity of wavelength λ = 970 nm (0.97 μm) is 3 W. The radiant energy is 90 joules. After laser treatment, a small amount of saline (0.2–0.5 mL) was injected. Determine the position of the elbow pin with the help of the image, and pull out the guide pin. Draw the elbow needle close to the fiber ring, and then enter the nucleus pulposus forward again until the same depth, repeat 3–5 times.

2.3. Imaging examination of pig intervertebral disc

Before modeling, 1 month after modeling and 1 month after the operation, MR examination was carried out respectively to observe the status of the intervertebral disc. Every time MR examination was carried out, pigs were given general anesthesia and vital signs were monitored. After MR, the diet and feces of pigs were closely observed for 3 days. When everything was normal, the pigs were fed in a unified way, and Pfirrmann grading system was used to evaluate the intervertebral disc.

2.4. Segmentation method of intervertebral disc

2.4.1. Automatic statistical shape model

Suppose there are n shapes in the training set S, and each shape $S_i(i = 1,2,\ldots, N)$ can be represented by a one-dimensional vector, Because the number of points of each shape is not the same, 8 points of the intervertebral disc are selected as the main feature points (including 2 boundary corner points), and then all shapes in the training set are sampled according to the given initial arc length parameter set $\{\psi_i\}$ to obtain the same number of n feature points, and the N shapes are expressed as n * n-dimensional vector $\{X_i\}$. In order to eliminate the differences caused by displacement, angle and size, the general alignment method is used to align all the sampled shapes [14,15]. The dimension of $\{X_i\}$ is reduced by principal component analysis (PCA). The vector X_i corresponding to each shape S_i can be expressed by the following linear model:

$$\boldsymbol{X_i = \overline{X} + Pb_i = \frac{1}{N}\sum_{i=1}^{N} X_i + \sum_{s=1}^{n_p} p_s b_{s,i}} \tag{1}$$

$$\boldsymbol{-3\sqrt{\lambda_s} \leqslant b_s \leqslant 3\sqrt{\lambda_s}}$$

where: $\overline{X}$ is the average shape, P = $\{P_s\}$ is the eigenvector used to describe the shape transformation mode (corresponding to the eigenvalue $\{\lambda_s\}$), b_i = $\{b_{s,i}\}$ is the shape parameter used to control the shape transformation mode. n_p can be derived from the following formula:

$$\begin{cases} \boldsymbol{0 \leqslant \alpha \leqslant 1} \\ \boldsymbol{\sum_{i=1}^{n_p} \lambda_s / \sum_{j=1}^{N} \lambda_s > \alpha} \\ \boldsymbol{1 \leqslant n_p \leqslant N} \end{cases} \tag{2}$$

The value of α is usually greater than 0.90, and 0.98 is used in this experiment. Many experiments show that this value can ensure more kinds of principal components and effectively reduce the $\{X_i\}$ dimension.

In order to obtain an effective statistical shape model from the training set $\{S_i\}$, following the principle of Occam's razor that "simple description is the best", a standard for selecting the arc length parameter set $\{\psi_i\}$ is formulated, and the simplicity of the model is described by MDL as a quantitative method. The final objective function is as follows:

$$\boldsymbol{F_{MDL} = \sum_{i=1}^{n_b}\left(1 + \ln \sigma_i^2\right) + \sum_{j=1}^{n_l}\left(\ln \sigma_{max}^2 + \left(\frac{\sigma_j}{\sigma_{max}}\right)^2\right)} \tag{3}$$

$$\boldsymbol{n_b + n_1 = n_p}$$

where: n_b is the number of feature directions with larger eigenvalue / variance, n_l is the number of feature directions with smaller eigenvalue / variance, and σ is the variance of $b_{m,i}$ in the direction P_m.

The calculation of Eq (3) is very complicated. Thodberg proposed a simplified method to simplify the obje ctive function to

$$\boldsymbol{F_{MDL} = \sum_{m=1}^{n_p} \psi_m} \tag{4}$$

among

$$\boldsymbol{\psi_m = \begin{cases} 1 + \ln \beta, \beta \geqslant 1 \\ \beta, \beta < 1 \end{cases}}$$

$$\boldsymbol{\beta = \lambda_m / \lambda_{cut}}$$

In order to obtain the best statistical shape model, the arc length parameter set $\{\psi_i\}$ is selected by Eq (4). The process of automatic statistical shape modeling based on MDL is as follows

1) The shape set $\{S_i\}$ is obtained by extracting the disc shape from the training set.

2) The shape parameters are initialized, and the shape set $\{S_i\}$ is sampled according to the initial arc length parameter set $\{\psi_i\}$ to get the shape feature point vector set $\{X_i\}$.

3) All shapes are aligned by the general analysis (updating the attitude parameters p (s, θ, t), s

for size, θ for angle, t for displacement).

4) PCA method was used to reduce dimension.

5) Calculate the value of the objective function F_{MDL}: if it converges, skip to step 6; otherwise, update the feature point distribution and repeat Steps 3–5).

6) The final statistical shape model expression is obtained.

2.4.2. 2D local gradient model

In order to make the model boundary closer to the real contour, the simplest method is to segment the strongest boundary along the contour. However, model points are not always on the strongest boundary, they may be on the second strongest boundary or other locations. The solution to this problem can be achieved by learning knowledge from training. Learning knowledge from the training set, constructing local gradient model and adding local statistical gradient model into ASM can improve the performance of ASM.

In order to improve the robustness and efficiency of image segmentation, a local gradient model is established in a multi-scale framework. A Gaussian image pyramid is built for each gray image of the training set. The base image (level 0) is the original image (the bottom image). The method to obtain other levels of Gaussian image pyramid image is: smoothing high-resolution image, and sampling half pixels from each dimension to obtain low resolution image. 1D local gradient model has limitations, only samples the pixels on the normal, the local gradient model is not robust enough, so 2D local gradient model can improve the robustness of the model.

On each layer of Gaussian pyramid image, a rectangular region pixel is sampled along the contour for each feature point. The rectangular region is shown in Figure 1 (2H + 1 pixel is taken in the normal direction, 2f + 1 pixel is taken in the line direction of two points). The rectangular region pixels of each feature point can be represented by the matrix $g_i((2h+1)*(2f+1))$. In order to reduce the influence of gray change, the gray difference of adjacent pixels (along the normal direction) is recorded, and the samples are normalized to $\{g_i\}$:

$$\boldsymbol{g_i(k)} \rightarrow \frac{\boldsymbol{g_i(j_1,k)-g_i(j,k)}}{\sum_{\boldsymbol{j=1}}^{\boldsymbol{2h}} \boldsymbol{|g_i(j+1,k)-g_i(j,k)|}} \tag{5}$$

where: $g_i(k)$ is the value of the k-th column of g_i, and $g_i(j,k)$ is the value of the k-th column of the j-th row of the vector g_i. Assuming that they follow a multivariate Gaussian distribution, the 2D local gradient model can be obtained as follows:

$$\boldsymbol{f(g_n)} = \boldsymbol{(g_n - \sum_{i=1}^{n_s} g_i)^T cov(\{g_i\})^{-1}(g_n - \sum_{i=1}^{n_s} g_i)} \tag{6}$$

where g_n is the matching value of the new sample. Figure 1 show the sampling principle of local gradient model.

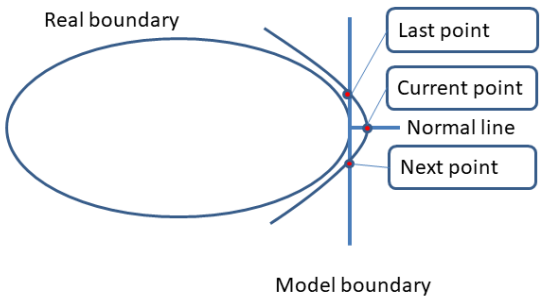

Figure 1. Sampling principle of local gradient model.

2.4.3. Segmentation

The segmentation of 2D-AASM method includes two parts: locating the initial contour and searching the final contour by 2D-AASM model. The position of the initial contour will seriously affect the final segmentation result, so it should be consistent with the target contour as much as possible. The method of locating the initial contour: manually select two corners in the test image, align the average shape of the model with it automatically, and the aligned average shape is used as the initial contour. Considering the geometric characteristics of the intervertebral disc, this method can get the initial contour which is very close to the target contour. In the 2D-AASM model, multi-scale search method is used to search from the low resolution layer to the original image. The steps of 2D multi-scale search algorithm are as follows:

1) For PL = $PL_{max} \rightarrow 0$ (PL_{max} is the maximum number of pyramid layers).

a) The initial boundary points of PL layer are calculated.

b) The rectangular region m (m = (2 (k-h) + 1) * (2f + 1) of each feature point is sampled on the image, and k is the number of sampled pixels along the normal direction).

c) The attitude parameter p (s, θ, t) and shape parameter b are updated to adjust the model to a new point.

d) Repeat a) and b) until the point beyond n_{close} is very close to the target position, or N_{max} iterations of this layer have been completed (n_{close} is the percentage of convergence points, 98% in the experiment, N_{max} is the number of iterations allowed for each layer, 40 in the experiment).

e) PL→PL-1

2) After converging on level 0, the final result is obtained according to the parameters.

2.5. Specimen collection and detection

Two months later, the three groups of pigs were treated with bloodletting from carotid artery. The corresponding intervertebral discs were dissociated, the fibrous rings were taken out and stored in a refrigerator at -80 ℃, and then the expression of APQ-1 was detected by Western Blot, and the intervertebral discs (L2-3, L3-4, L4-5 and L5-6 of each pig) were taken, together with the upper and lower part of the vertebral body. The tissue samples were fixed with 10% formaldehyde. The intervertebral discs were decalcified with EDTA solution. The discs were dehydrated, transparent and embedded, and were sectioned continuously at 5 μm cross section. HE staining was used to observe the intervertebral discs in each midsagittal plane, and the images were taken.

2.6. Statistical analysis

SPSS 19.0 software was used for statistical analysis. The experimental data were expressed as mean ± standard deviation ($\bar{x}$ ± SD). One way Analysis of Variance was used for comparison between groups. Analysis of variance in repeated measurement design was used for comparison within groups. The nonparametric test was used to compare the grade data. The difference was statistically significant ($P < 0.05$).

3. Results

3.1. Intervertebral disc segmentation

The quantitative comparison of shape models established by different modeling methods was shown in Table 1. The proposed automatic modeling method is better than manual method and arc length parameter method, and has smaller mode variance and objective function value, which can shorten the modeling time and reduce the cost of long-time work. Thus, the a simple and effective model was easy to establish. The results of different models for intervertebral disc segmentation were shown in Figure 2. The 2D-AASM method was more accurate than the other two methods. The quantitative comparison of segmentation results is given in Table 2. The over segmentation rate, under segmentation rate and Dice coefficient data show that the proposed method is better and more stable than the traditional ASM method and 1D-ASM method.

Table 1. Quantitative comparison of manual, arc length parameters and automatic modeling methods.

Model	manual	arc length parameters	automatic
1	0.0043	0.0044	0.0041
2	0.0013	0.0014	0.0011
3	0.0004	0.0005	0.0003
Total variance	0.0058	0.0063	0.0052
objective function	63.8835	79.3742	61.4268

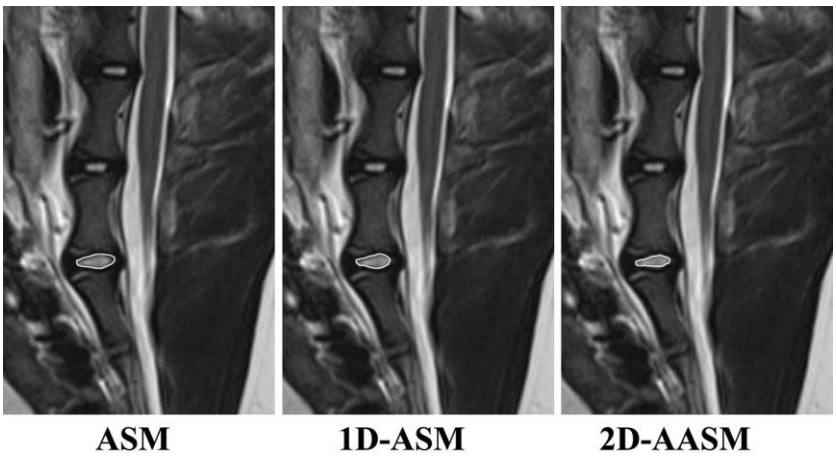

Figure 2. Intervertebral disc segmentation by different models.

Table 2. Comparison of traditional ASM, 1D-ASM and 2D-AASM search results (%).

Methods	*Dice*	*TPF*	*FNF*	*FPF*	*TNF*
ASM	87.38	75.62	23.17	0.09	99.82
1D-ASM	91.49	92.83	6.62	0.21	99.78
2D-AASM	97.72	99.14	0.83	0.04	99.75

3.2. Imaging observation

The model established by the proposed method is more accurate and the segmentation result is more accurate. As shown in Figure 3, in the con group, the fibrous ring of intervertebral disc showed moderate signal, and the nucleus pulposus showed high signal shadow. The fiber ring signal was slightly uneven, and the local signal was low; In the mod group, the intervertebral space became narrowed, the disc was retrogressive, the dural sac was compressed, the signal of nucleus pulposus was basically lost, and the disc was transformed; In the Las group, the spinal morphology also showed some degenerative changes, the nucleus pulposus showed medium high signal, the disc appeared certain deformation, the signal was partially missing, some areas showed low signal shadow, but it was basically complete, because of the great tissue damage during the modeling process, the height of some vertebrae changed significantly.

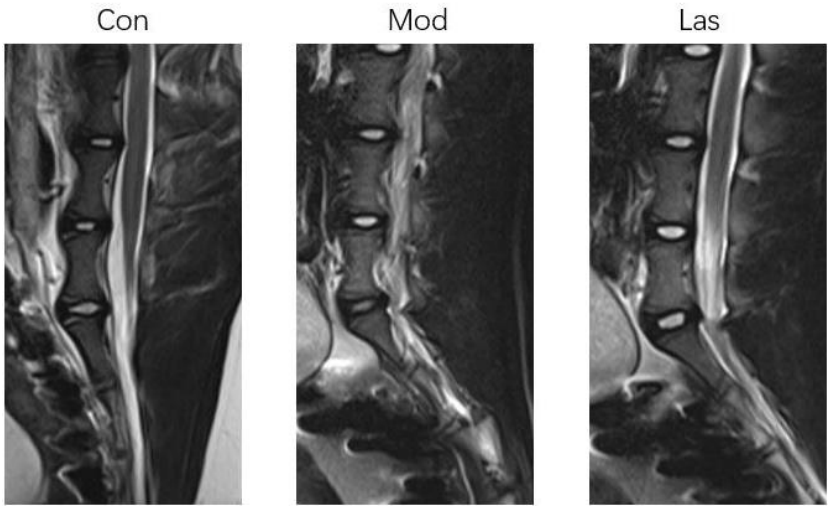

Figure 3. MRI comparsion of intervertebral discs of Bama miniature pigs.

The results of imaging classification were shown in Table 3. MR images in Con group were all grade I ~ II, no obvious signs of degeneration were found; in the Mod group, the main grade was III ~ IV, with obvious degeneration; in Las group, grade II ~ III was the main grade, and the degeneration was mild; the total number of grade I and II in Con group was 100%, that in Mod group was 16.7%, and that in Las group was 66.7%. The nonparametric test showed that there was statistical difference between the groups ($Z = 24.256$, $P < 0.001$).

Table 3. Intervertebral disc imaging grading table.

Group	Number of discs	Grade I	Grade II	Grade III	Grade IV
Con	12	10	2	0	0
Mod	12	0	2	3	7
Las	12	1	7	3	1

3.3. Histomorphological changes of porcine intervertebral disc

Visual observation of the intervertebral disc tissue showed that there was no obvious degeneration of the intervertebral disc in the Con group, the nucleus pulposus was white jelly like, with a lot of water content and a clear structure. There was a clear boundary between the fibrous ring and the nucleus pulposus. The fibrous ring structure was clear and arranged in concentric circles. Thompson's grade was grade I; in the Mod group, obvious signs of degeneration in the disc were found, obvious rupture zone was appeared in the fibrous ring, and a scar like acupuncture channel running through the whole fibrous ring and nucleus pulposus, with hardening around. Thompson classification was divided into III ~ IV grades; in the Las group, the disc thickness decreased, the interstitial component decreased, the nucleus pulposus was gray white, the boundary between the fibrous ring and nucleus pulposus was slightly fuzzy, and white fibrous tissue appeared around the nucleus pulposus, Thompson’s grade was II ~ III (Figure 4). The nonparametric test also showed that there was statistical difference between the groups ($Z = 25.665$, $P < 0.001$).

Figure 4. Gross pathological changes of plate among the three group.

HE staining showed that the structure of intervertebral disc in Con group was clear, the cartilage matrix was rich, the shape was clear, the cells were arranged orderly, the nucleus was small, round, located in the center, and the structure of fibrous ring was normal; in the Mod group, the tissue structure was disordered, the collagen fibers were enlarged and irregular, and there was inflammatory necrosis. The fiber was coarsened and glassy. The nucleus pulposus cells decreased, the fibers arranged disorderly, the layers were not clear, the collagen fibers were severely twisted, and some of them were broken. The number of cells decreased significantly, the nucleus increased, and the cells were between chondrocytes and fibrocytes; in Las group, there were fissures in the nucleus pulposus. The cell morphology changed, the cell structure was still clear, the arrangement was slightly

disordered, the cell number was medium, the ratio of nucleus to cytoplasm was basically normal, and there was slight inflammatory necrosis and exudation (Figure 5 and Table 4).

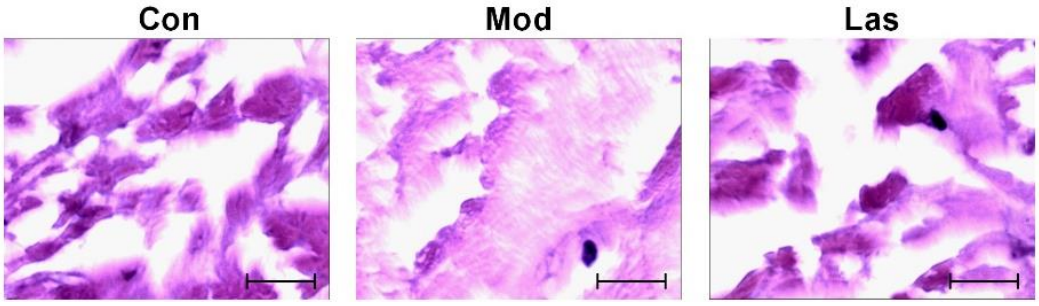

Figure 5. Histopathological changes of intervertebral discs.

Table 4. Pathological grading table of three groups of porcine intervertebral disc.

Group	Number of discs	Grade I	Grade II	Grade III	Grade IV
Con	12	12	0	0	0
Mod	12	0	2	3	7
Las	12	3	6	2	1

3.4. Changes of AQP-1 expression in intervertebral disc fibrosis

The results of immunohistochemistry showed that AQP-1 was positively expressed in the discs of Con group, and the cytoplasm was stained brown; in Mod group, there were almost no positive granules and the structure was disordered; in Las group, part of the expression staining was obviously weakened, and the number of positive cells was significantly reduced compared with Con group, but significantly increased compared with Mon group, as shown in Figure 6.

Western results showed that compared with Con group, AQP-1 expression in Mod group and Las group decreased significantly ($P < 0.05$); compared with Mod group, AQP-1 expression in Las group increased significantly ($P < 0.05$, see Figure 7).

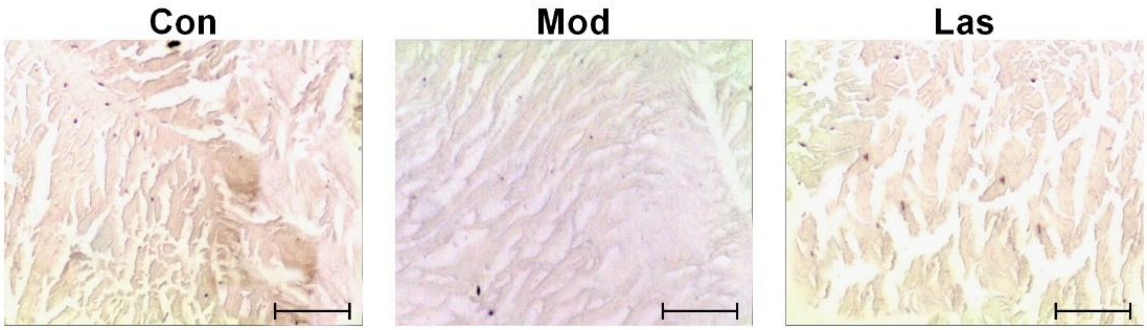

Figure 6. AQP-1 change among three groups.

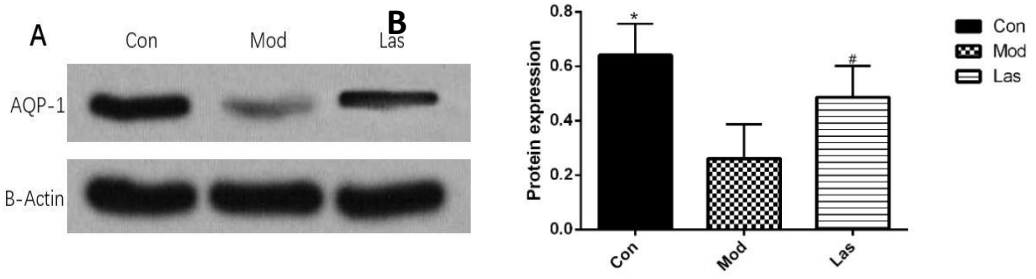

Figure 7. Results of AQP-1 Western Blot in three groups of Bama miniature pig intervertebral discs. (vs. Mod group and Las group, *P < 0.05; vs. Mod group, #P < 0.05).

4. Discussion

Low back pain caused by intervertebral disc degeneration is one of the common diseases in the world. There are many pathogenic factors of intervertebral disc degeneration, and its pathological mechanism is very complex. Its clinical symptoms include lumbago and leg pain, disc herniation, spinal stenosis and lumbar instability. The research shows that among the many pathogenic factors of lumbar disc degeneration, the abnormal nutrition and metabolism of lumbar disc nucleus is a very important factor [16]. The change of normal hydrodynamics function in the intervertebral disc is the common pathway leading to the degeneration of the disc. The pressure load of the disc changes, and the content of water in the disc changes with the change of the pressure. The normal intervertebral disc deforms in the process of continuous movement, and the speed of water flowing in and out of the disc is very fast. The fibrous ring is a dense ring structure, which can not be fully explained by pure diffusion. Studies at home and abroad have found that AQPs are expressed in intervertebral discs, and AQPs play an important role in maintaining spinal stability, buffering and even distribution [17–19].

AQP is a group of membrane channel proteins related to transmembrane water transport, which mediates the transmembrane water transport of different types of cells. This channel not only penetrates water, but also some members of its family have certain selective permeability to glycerol and urea. In recent years, the transport of AQPs in the water and nutrients of disc cells has been recognized by more and more people. There are 13 AQPs subclasses found in mammals. AQP-1 is one of its important members. Its relative molecular mass is about 28 KD and it exists in the form of tetramer. AQP-1 is expressed in various tissues and participates in water transport [20,21]. Richardson et al. [22] found that AQP-1 was expressed in the human fibrous rings and nucleus pulposus, but not in the outer fibrous rings. The results showed that AQP-1 content decreased with the increase of disc degeneration [10,12,23].

At present, minimally invasive technology and high temperature thermocoagulation technology are relatively mature methods for the treatment of disc herniation, but this method may cause irreversible damage to the disc, which is difficult to ensure long-term effect. The low-intensity laser technology used in this paper is characterized by the formation of a number of small channels in the total volume of the disc less than 1% of the volume of the disc. Using 0.97 μm wavelength radiation, the multi-channel laser puncture for reconstruction and repair of intervertebral disc can significantly expand the indication range of percutaneous laser puncture for the treatment of lumbar disc derived diseases, and do not damage the structure of the disc itself to the greatest extent [24,25].

In this experiment, a clinical similar model of disc degeneration was made by a small Bama pig.

MR examination was carried out one month after the model was made. It was found that the intervertebral disc undergoing puncture had narrow space, backward process of disc, compression of dural sac, loss of signal of nucleus pulposus, deformation of fibrous ring and other changes. According to the Pfirrmann grading standard, the treated intervertebral disc was in grade III - IV, indicating that the model was successful. One month after the successful establishment of the model, the low-intensity laser treatment was carried out. The results showed that the MRI Pfirrmann classification of the intervertebral disc in the Las group was significantly lower than that in the Mod group. The results of cadaver specimen and HE staining also confirmed that the degenerative lesions of the intervertebral disc in the Las group were significantly reduced, suggesting that the low-intensity laser has a certain repair function on the intervertebral disc. In addition, low-intensity laser stimulates the surrounding tissues in the form of biological waves, which reduces the damage to the surrounding intervertebral disc in the process of treatment. The results of immunohistochemistry showed that AQP-1 was significantly positive in the Con group, and the cytoplasm was stained brown; there were almost no positive granules in the Mod group, and the structure was disordered; in the Las group, part of the expression staining was significantly weakened, and the number of positive cells was significantly reduced compared with the Con group, but significantly increased compared with the Mod group. Western results showed that, compared with the Con group, the AQP-1 expression in the Mod group and Las group decreased significantly ($P < 0.05$); compared with the Mod group, the AQP-1 expression in the Las group increased significantly, which indicated that the low-intensity laser had a certain repair function on the intervertebral disc. One of the mechanisms may be to increase the expression of AQP-1, which is closely related to transport and nutrition metabolism, to restore the input of nutrients and the output of metabolic waste, to effectively alleviate the degeneration of the disc, and even to repair the degenerated disc.

5. Conclusions

In conclusion, the 2D-AASM method effectively improves the accuracy of intervertebral disc segmentation. The low-intensity laser repair can be used to treat degenerative disc through biological wave, which has certain protection and repair effect on degenerative disc. Its mechanism may be related to up-regulation of AQP-1, but there are many mechanisms need to be further confirmed.

Acknowledgments

The study was supported by the Key Program of Natural Science Foundation of Liaoning Province (No: 20170540943).

Conflict of interest

The authors declared that there was no conflict of interests.

References

1. N. Newell, J. P. Little, A. Christou, M. A. Adams, C. J. Adam, S. D. Masouros, Biomechanics of the human intervertebral disc: A review of testing techniques and results, *J. Mech. Behav. Biomed. Mater.*, **69** (2017), 420–434.

2. D. C. Noriega, F. Ardura, R. Hernández-Ramajo, M. Martín-Ferrero, I. Sánchez-Lite, B. Toribio, et al., Intervertebral disc repair by allogeneic mesenchymal bone marrow cells: a randomized controlled trial, *Transplantation*, **101** (2017), 1945–1951.
3. J. Stergar, L. Gradisnik, T. Velnar, U. Maver, Intervertebral disc tissue engineering: a brief review, *Bosn. J. Basic. Med. Sci.*, **19** (2019), 130–137.
4. M. P. van den Heuvel, L. H. Scholtens, R. S. Kahn, Multiscale neuroscience of psychiatric disorders, *Biol. Psychiatry.*, **86** (2019), 512–522.
5. Y. Yang, J. Wang, C. Xu, Intervertebral disc segmentation and diagnostic application based on wavelet denoising and AAM model in human spine image, *J. Med. Syst.*, **43** (2019), 275.
6. A. D. Diwan, H. K. Parvataneni, S. N. Khan, H. S. Sandhu, F. P. Girardi, F. P. Cammisa, Current concepts in intervertebral disc restoration, *Orthop. Clin. North. Am.*, **31** (2000), 453–464.
7. Z. Peng, W. Zhao, S. Hu, Computer three-dimensional reconstruction and pain management for lumbar disc herniation treated by intervertebral foramen endoscopy, *J. Med. Image Health Int.*, **9** (2019), 1776–1781.
8. A. G. Nerlich, E. D. Schleicher, N. Boos, 1997 Volvo award winner in basic science studies, immunohistologic markers for age-related changes of human lumbar intervertebral discs, *Spine*, **22** (1997), 2781–2795.
9. M. A. Rivera, T. D. Fahey, Association between aquaporin-1 and endurance performance: a systematic review, *Sports Med. Open*, **5** (2019), 40.
10. U. Taş, S. Caylı, A. Inanır, B. Ozyurt, S. Ocaklı, Z. Karaca, et al., Aquaporin-1 and aquaporin-3 expressions in the intervertebral disc of rats with aging, *Balkan Med. J.*, **29** (2012), 349–353.
11. J. Badaut, F. Lasbennes, P. J. Magistretti, L. Regli, Aquaporins in brain: distribution, physiology, and pathophysiology, *J. Cereb. Blood Flow Metab.*, **22** (2002), 367–378.
12. H. Hoffman, A. W. Choi, V. Chang, J. Kimball, S. V. A, R. Virani, et al., Aquaporin-1 expression in herniated human lumbar intervertebral discs, *Global Spine J.*, **7** (2017), 133–140.
13. H. Xie, Y. Jing, J. Xia, X. Wang, C. You, J. Yan, Aquaporin 3 protects against lumbar intervertebral disc degeneration via the Wnt/β-catenin pathway, *Int. J. Mol. Med.*, **37** (2016), 859–864.
14. D. Oriola, F. Jülicher, J. Brugués, Active forces shape the metaphase spindle through a mechanical instability, *Proc. Natl. Acad. Sci. USA*, **117** (2020), 16154–16159.
15. A. G. Warrener, Hominin hip biomechanics: changing perspectives, *Anat Rec (Hoboken)*, **300** (2017), 932-945.
16. Y. J. Liu, G. S. Huang, C. J. Juan, M. S. Yao, W. P. Ho, W. P. Chan, Intervertebral disk degeneration related to reduced vertebral marrow perfusion at dynamic contrast-enhanced MRI, *Am. J. Roentgenol.*, **192** (2009), 974–979.
17. U. Tas, S. Cayli, A. Inanir, B. Ozyurt, S. Ocakli, Z. I. Karaca, et al., Aquaporin-1 and aquaporin-3 expressions in the intervertebral disc of rats with aging, *Balkan Med. J.*, **29** (2012), 349–353.
18. H. Sakai, K. Sato, Y. Kai, T. Shoji, S. Hasegawa, M. Nishizaki, et al., Distribution of aquaporin genes and selection of individual reference genes for quantitative real-time RT-PCR analysis in multiple tissues of the mouse, *Can. J. Physiol. Pharmacol.*, **92** (2014), 789–796.
19. J. W. Snuggs, R. E. Day, F. C. Bach, M. T. Conner, R. A. D. Bunning, M. A. Tryfonidou, et al., Aquaporin expression in the human and canine intervertebral disc during maturation and degeneration, *JOR Spine*, **2** (2019), e1049.

20. A. Mobasheri, E. Trujillo, S. Bell, S. D. Carter, P. D. Clegg, P. Martin-Vasallo, et al., Aquaporin water channels AQP1 and AQP3, are expressed in equine articular chondrocytes, *Vet. J.*, **168** (2004), 143–150.
21. W. D. Stamer, R. W. Snyder, B. L. Smith, P. Agre, J. W. Regan, Localization of aquaporin CHIP in the human eye: implications in the pathogenesis of glaucoma and other disorders of ocular fluid balance, *Invest. Ophthalmol. Vis. Sci.*, **35** (1994), 3867–3872.
22. S. M. Richardson, R. Knowles, D. Marples, J. A. Hoyland, A. Mobasheri, Aquaporin expression in the human intervertebral disc, *J. Mol. Histol.*, **39** (2008), 303–309.
23. S. B. Li, K. S. Yang, Y. T. Zhang, Expression of aquaporins 1 and 3 in degenerative tissue of the lumbar intervertebral disc, *Genet. Mol. Res.*, **13** (2014), 8225–8233.
24. D. M. Elliott, J. J. Sarver, Young investigator award winner: validation of the mouse and rat disc as mechanical models of the human lumbar disc, *Spine*, **29** (2004), 713–722.
25. S. O. Sierra, A. M. Deana, S. K. Bussadori, A. C. da Mota, L. J. Motta, R. A. Ferrari, et al., Effect of low-intensity laser treatment on pain after extraction of impacted mandibular third molars: a randomised, controlled, clinical trial, *Br. J. Oral. Maxillofac. Surg.*, **53** (2015), 996–1000.